SYNTHESIS OF MESOPOROUS HYDROXYAPATITE THROUGH A SOFT TEMPLATE ROUTE USING NON-IONIC SURFACTANT

Wee-Keat Cheah, Chin-Wei Ooi, Radzali Othman, and Fei-Yee Yeoh

School of Materials and Mineral Resources Engineering, Universiti Sains Malaysia, Penang, Malaysia, Tel: 604 599 6175, e-mail: srfeiyee@eng.usm.my

Received Date: January 9, 2012

Abstract

Conventional synthesis of mesoporous hydroxyapatite (HAp) commonly employs co-precipitation method using cationic surfactants such as CTAB. Such surfactants are expensive and create tinier mesopores without an interconnecting pore structure. Using non-ionic surfactants in the synthesis of mesoporous HAp, the pore formation could be induced to tailor desirable pore characteristics. This paper reports on synthesis of mesoporous HAp through soft template route using non-ionic surfactants P123, F127 and P123/F127. Calcination was carried out at 550 °C for 6 hours to reveal pores through the removal of the organic surfactant. The formation of HAp prior and subsequent to the calcination was evaluated through several materials characterization techniques. The X-ray diffraction (XRD) diffractograms revealed characteristic peaks of HAp corresponds to a typical HAp crystal phase, whereby a hexagonal lattice structure was deduced. SEM micrographs revealed rod-like HAp particles with diameter of approximately 24 nm and length ranging from 100 nm. TEM revealed the formation of nanopore channels within the rod-like structure, aligned in a lengthwise direction within the rods. The nanopore channels were consistent with the cavities being generated by the removal of non-ionic surfactant. The pores formed were found to be randomly distributed within the HAp structure.

Keywords: F127, Mesoporous Hydroxyapatite, P123, Pluronics, Triblock co-polymer

Introduction

Synthetic hydroxyapatite (HAp), $Ca_{10}(PO_4)_6(OH)_2$, has garnered quite some attention owing entirely to its similar phase, structure and chemical composition as that of the human bones and teeth [1]. Due to these similarities, HAp is often targeted to be used as bone implants and implant coatings [2-4].

The porous variant of HAp, mesoporous HAp in particular, has a great potential to be used as drug delivery carriers especially for bone-related diseases [5-6]. Take for example, the anti-tumor and antibiotics used for treating osteomyelitis, a bone infection; mesoporous HAp can be used for the delivery of the mentioned drugs [6]. However, before a mesoporous HAp is to be used as a delivery carrier for a specific drug, the suitability as a drug delivery agent against the pore characteristics of mesoporous HAp has to be determined. In a study by Descamps and collogues, the drug loading and the drug release rates of mesoporous HAp pellets were tested with gentamicin antibiotic, an antibiotic typically used in osteomyelitis treatments [7]. The study revealed that the as-prepared porous HAp pallets are effective in delivering the antibiotic to the intended sites, at which a progressive release is achieved for over a long period of time. In order to achieve this condition, the selected drug has to be paired off with mesoporous HAp with a suitable or matching pore characteristic; that is the pore shape, pore size and porosity. Aside from the matching pore characteristics, mesoporous HAp for drug delivery should possess a crystal structure with lowered crystallinity unlike HAp intended implant applications, since a lowered crystallinity would result in higher dissolution rate [8-9].

HAp drug delivery agents with better dissolution rates would be beneficial since carriers are no longer required once the drugs are released at the targeted site.

With the development of more drugs at present, specifically drugs targeting bone infections and diseases, a wide range of suitable mesoporous HAp with various pore characteristics would be needed [10]. Thus, processes to produce mesoporous HAp with controlled pore characteristics has to be established to cater for the developed drugs targeting bone infections and diseases.

There are various well-known methods to produce HAp; co-precipitation method [11], hydrothermal method [12] and mechano-chemical method [13], just to name a few. Among these methods, the co-precipitation method has certain advantages in the sense that this method is simple and straight-forward, while the cost of production is low [6]. A direct mixture of pore forming agent (template), calcium ion (Ca^{+}) and phosphate ion (PO_4^{3-}) sources along with the standard co-precipitation procedures would generally produce mesoporous HAp [14].

However, in the synthesis of mesoporous HAp, the limitations of the co-precipitation method are obvious. In order to produce pores in mesoporous scale, soft template ionic surfactants such as CTAB are commonly used as the pore forming agents [15]. Ionic surfactants are difficult to be removed from the mesoporous HAp using the co-precipitation method [16]. Taking cationic surfactant CTAB as an example, the formation of ordered mesopores are derived from the CTAB-PO_4^{3-} (PO_4^{3-} = ion from phosphate source) mixture, forming rod-like micelles in the process. The formation of CTAB-PO_4^{3-} would require a specific template removal process for the formation of mesopores [6]. Non-ionic surfactants such as triblock co-polymers Pluronics on the other hand, are less affected by the concentration and nature of electrolytes present in the said mixture, when compared to ionic surfactants [17]. Pore characteristics of mesoporous HAp could be better controlled through the variation of parameters such as the non-ionic surfactant chain length [14].

Hence, Pluronics P123 and F127 were incorporated into the synthesis of mesoporous HAp to evaluate the resulting pore characteristic of each synthesized sample. On top of that, mesoporous HAp utilizing a combination of both Pluronics P123 and F127 was also synthesized and evaluated.

Materials and Methods

Preparation of Mesoporous HAp Powder

Table 1. Chemicals

Chemical	Chemical Formula	Manufacturer (Code)	Country
Sodium dihydrogen phosphate dihydrate	NaH2PO4.2H2O	Merck (6345)	Germany
Pluronic (P123, F127)	PEOm-PPOn-PEOm	BASF	Germany
Calcium chloride dihydrate	CaCl2.2H2O	R&M (6880-00)	USA
Sodium hydroxide	NaOH	Merck (1823)	Germany

Mesoporous HAp powders were synthesized using three groups of non-ionic triblock co-polymers Pluronic as templates; P123 ($EO_{20}PO_{70}EO_{20}$), F127 ($EO_{100}PO_{65}EO_{100}$) and P123+F127, with EO denoting ethylene oxide and PO denoting propylene oxide. The powdered samples were prepared via a co-precipitation method. In this study, co-precipitation method was used to synthesize mesoporous HAp precursor powder. This method is modified from the one used by Zhao and Ma [14].

For sample P123-B (*B denoting before calcination*), 20 g of P123 and 5.881 g (0.04 mol) of calcium chloride dihydrate ($CaCl_2.2H_2O$) were dissolved in 200 ml of distilled water. The mixture was stirred briskly to obtain a clear micellar solution. The source of phosphate ion was prepared by dissolving 3.744 g (0.024 mol) of sodium dihydrogen phosphate dihydrate ($NaH_2PO_4.2H_2O$) in 60 ml of distilled water. Next, the phosphate ion containing solution was added with sodium hydroxide 1M to obtain a resulting solution with pH 12. Subsequently, the prior prepared mixture of P123 and calcium ion containing solution was slowly titrated with the phosphate ion containing solution, while maintaining a constant stirring motion until a milky suspension was yielded. The resulting mixture was then aged at room temperature (RT) for 24 h. Samples obtained were then centrifuged at 3000 rpm for 15 minutes. Resulting white precipitate was washed with excess distilled water to remove the remaining free ions such as Na^+ and Cl^-. Subsequently, the resulting as-synthesized white powders were dried in an oven at 100 °C for 24 h. Finally, the white powders were calcined at 550 °C for 6 hours to create pores by burning off the organic template, producing P123-C (*C denoting sample after calcination*).

The entire procedure above was repeated with 2 other variations of Pluronic surfactants (F127; P123+F127) to produce F127-B, F127-C, P123/F127-B and P123/F127-C. Table 2 summarizes the matrix of this experiment. Aside from the variation of Pluronics surfactant used, all other parameters remains unchanged.

Table 2. Matrix of Experiment

Pluronics Surfactant	Amount of Surfactant	Precursor Powder	Calcined Powder
P123	20 g	P123-B	P123-C
F127	20 g	F127-B	F127-C
P123/F127	10 g/10 g	P123/F127-B	P123/F127-C

Characterization of Mesoporous HAp Powder

The phases of the as-synthesized mesoporous HAp powdered samples were characterized using Bruker AXS D8, through a range of Bragg angles using a CuKα radiation (λ = 0.15406 nm). Fourier Transform Infrared Spectroscopy (FTIR) analysis technique was done with Perkin Elmer Spectrum One using KBr pellet method. Surface morphology of as-synthesized samples were examined with a field emission scanning electron microscope (FESEM) model Zeiss SUPRA 35VP FESEM, within magnification of 30,000 times and electron beam energy of 3 to 5 kV. Transmission electron microscopy (TEM) was carried out to the pore characteristic and particle morphology using TEM model Philips CM12. Additionally, Micromeritics ASAP 2000 gas adsorption analyzer was used to determine the specific surface areas [Brunauer–Emmett–Teller (BET) method] and pore size distributions [Barret-Joyner-Halenda (BJH) method from the desorption branch of the isotherm].

Results and Discussion

The crystal structure and phases of the synthesized samples, in a dried precursor state (P123-B, F127-B, P123/F127-B) and calcined state (P123-C, F127-C, P123/F127-C) were determined using XRD, as shown in Figure 1. The XRD results show that the phase of the precursor and calcined powders were quite consistent in which HAp phase was obtained, in comparison to PDF Number 09-0432. There was no obvious formation of intermediates such as tricalcium phosphate. The diffractograms in Figure 1 show typical diffraction peaks of HAp, especially the three distinctive peaks of HAp at 2θ = 25.88˚, 31.88˚ and 32.98˚, which can be indexed as (002), (211) and (300) respectively according to the standard International Centre for Diffraction Data (ICDD) reference data. The diffractograms also reveal that the structure of as-synthesized HAp belongs to the hexagonal P63/m space group with lattice constant of a and b = 9.418Å and c = 6.884Å. Calcined samples (P123-C, F127-C and P123/F127-C) produced similar patterns with slightly sharper peaks, indicating higher crystallinity with calcination process.

From the XRD diffractograms, crystallite size (X_S) of samples were calculated from the full-width half-maximum (FWHM) of diffraction peak (002) and summarized in Table 3. The crystallite sizes generally increases subsequent to the calcination process. The increase in temperature during the calcination process not only removes the organic surfactant template, but also causes the growth of HAp crystals. Generally, only a small difference in crystallite size is observed for the samples synthesized using different surfactant.

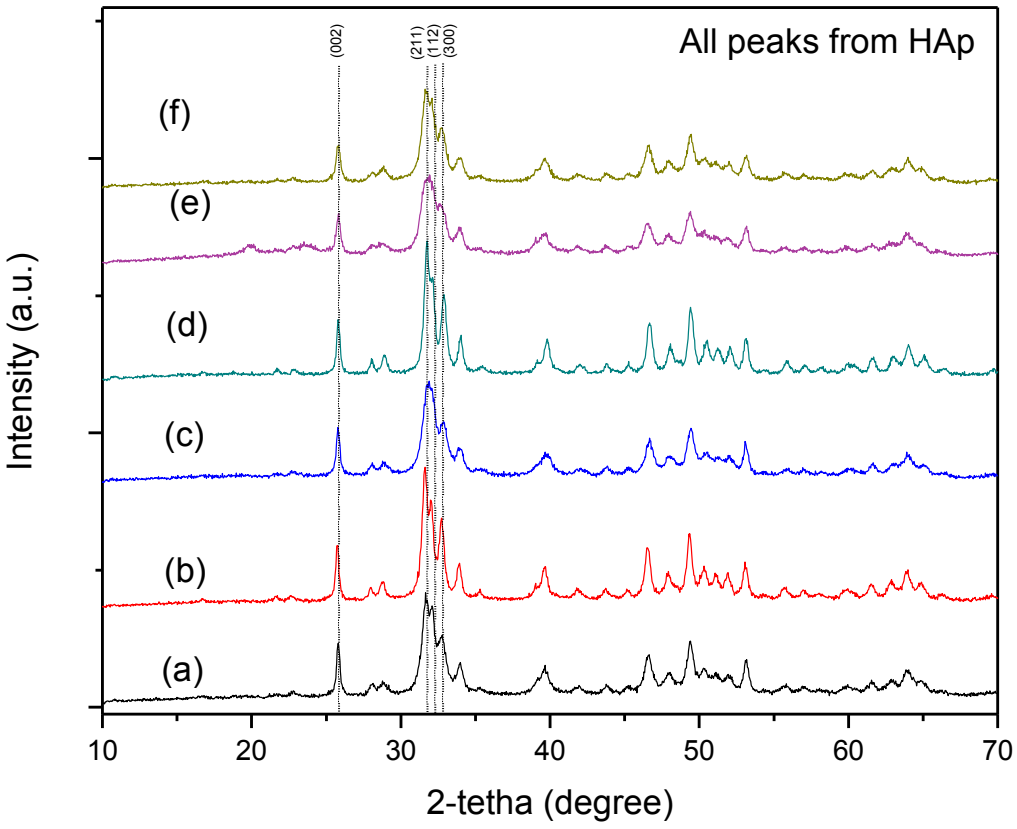

Figure 1. XRD patterns of HAp precipitate (a) P123-B, (b) P123-C, (c) F127-B, (d) F127-C, (e) P123/F127-B, and (f) P123/F127-C

Table 3. Crystallite Size Calculated from (002) Peak

Surfactant	Crystallite Size, XS (nm)	
	Before Calcination	After Calcination
F127	26.4	37.5
P123	24.1	30.9
P123/F127	22.9	24.8

The existence of surfactants did not induce the crystallization of other phases as the XRD patterns indicate this has not occurred since the lattice dimensions are in exact agreement with standard ICDD reference data; nor did the calcination process. The non-interaction of surfactants with the HAp crystal structure during calcination could be further supported with the FTIR spectra of P123-B and P123-C in Figure 2. The FTIR spectra of P123-B and P123-C is generally similar to the spectra of HAp synthesized with surfactants F127 and P123/F127 since all peaks present are accounted for. Peaks associated to the phosphate and hydroxyl groups present in HAp are observed in spectra of all samples (before and after calcination). The peaks labeled in Figure 2 are present prior to the calcination process were subsequently removed. H_2O peaks correspond to the adsorbed water on the HAp surface, were not observed after calcination. CH_3 (found in both PPO and PEO) and CH_2 (found in PPO) groups detected before the calcination process are from the organic surfactant templates. These groups are no longer present in calcined samples since all organic species were burnt off during the calcination process. Carbonates present in the HAp samples as a result of CO_2 incorporation during the synthesis [18] were converted back to carbon dioxide during the calcination process. In short, the crucial calcination step which is required for the removal of organic surfactant template did not result in any change in HAp crystal structure. Furthermore, there was no surfactant remaining in the sample subsequent to the calcination process, indicating complete removal of surfactant from the HAp samples.

Though the existence of surfactants does not affect the crystal structure, a mixture of surfactants P123 and F127 lowered the crystallinity, slightly dull peaks as observed in Figure 1 (e) & (f), in comparison to samples synthesized using single surfactant. Controlled reduction in crystallinity of sample P123/F127-C should prove to be a better drug delivery agent with the increased HAp dissolution rate. Mesoporous HAp derived using single surfactants P123 and F127 with higher crystallinity might result in detrimental effects if used as drug delivery agents since these carriers are still present on-site in the system even after the drug has been released.

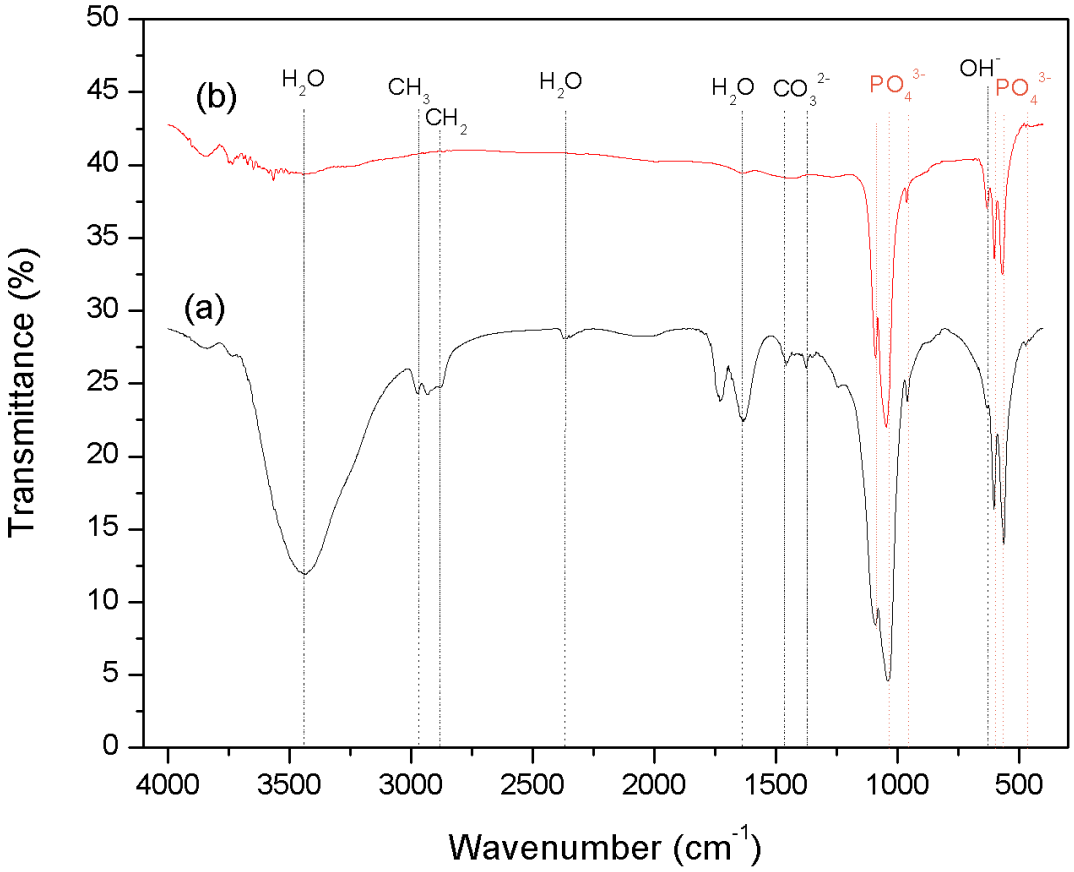

Figure 2. FTIR spectra of sample (a) P123-B and (b) P123-C

Morphologies of various synthesized mesoporous HAp samples were observed to be different in terms of length and diameter of rods. Figures 3 to 5 show the micrographs of HAp before and after calcination, produced by surfactants P123, F127 and P123/F127 respectively. In general, morphologies of the samples before calcination are observed to possess cotton-like shape. Morphologies of samples after calcination on the other hand are observed to possess rod-like particles with average length and diameter of approximately 100 nm and 24 nm respectively. Calcined samples show sharper and more distinct particles. Surface of calcined samples seems to be homogeneous and regular, without obvious ridges. HAp synthesized with P123 has thicker and shorter particles while HAp synthesized with F127 has thinner and longer particles. Mesoporous HAp synthesized with surfactant P123 + F127 however, is observed to possess thinner, longer particles and also thicker, shorter particles. The irregularity of particle shape is mainly due to non-homogeneous mixing of F127 and P123 micelles, thus causing a random interaction of surfactants and HAp.

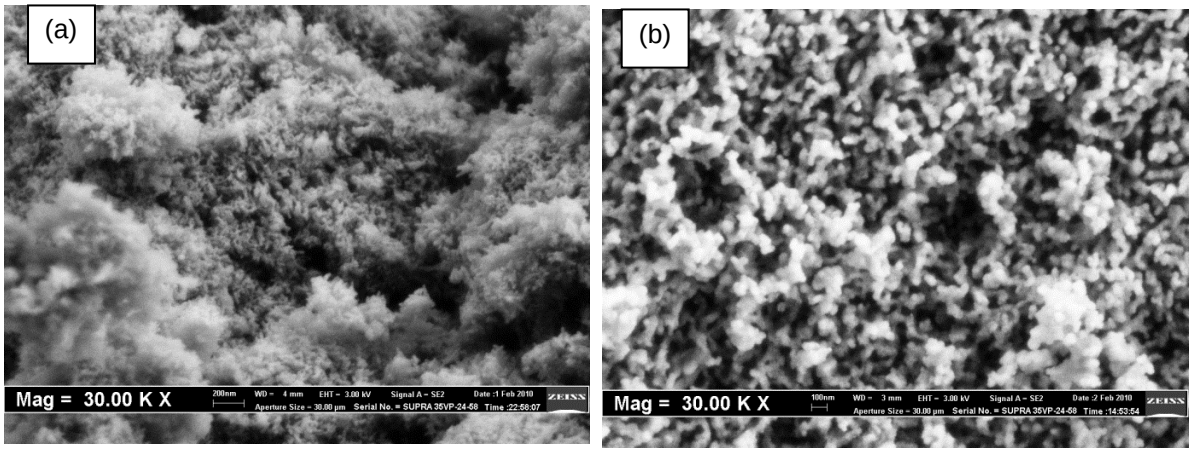

Figure 3. SEM micrographs of (a) P123-B and (b) P123-C

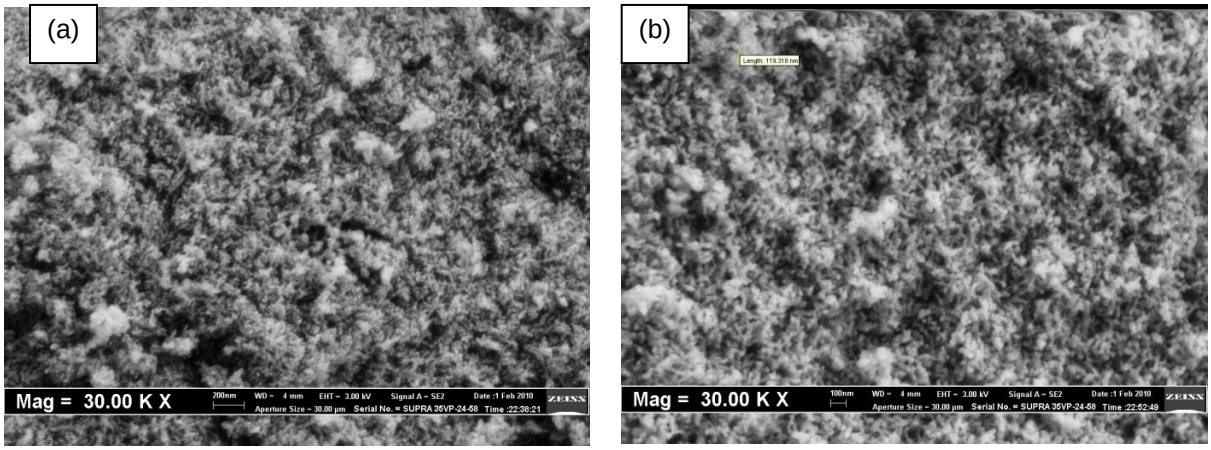

Figure 4. SEM micrographs of (a) F127-B and (b) F127-C

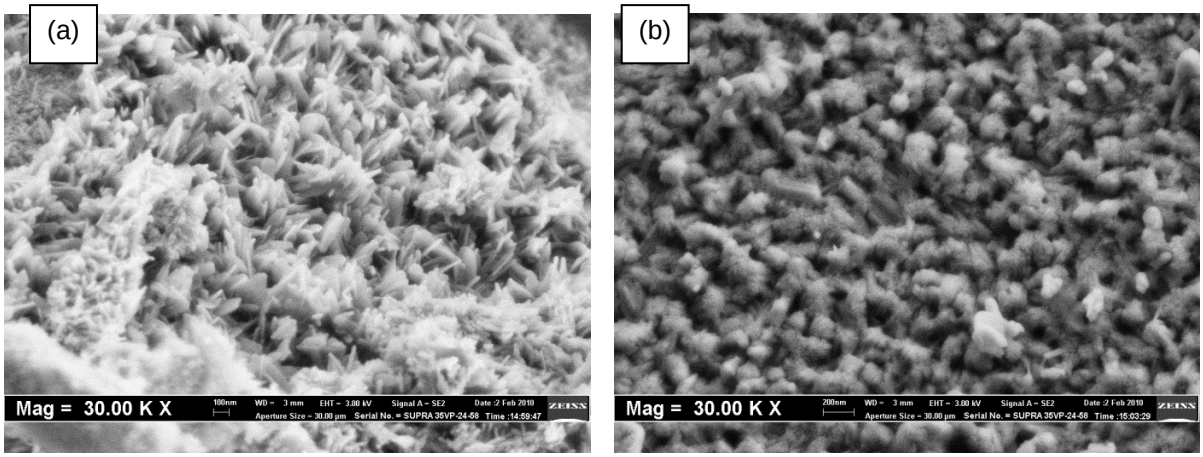

Figure 5. SEM micrographs of (a) P123/F127-B and (b) P123/F127-C

The presence of mesopores derived from the different surfactants was confirmed using high resolution TEM. Figures 6 to 8 clearly reveal the existence of mesopores within P123-C, F127-C and P123/F127-C particles after calcination. Figure 9 shows the two distinctive views of synthesized mesoporous HAp, from both axial and parallel views. The shaded fringes represent the boundaries of nano-channels formed within the rod-like HAp particle. These nano-channels are aligned in the lengthwise direction within the rod particles, and are consistent with the cavities generated by the removal of organic surfactant during calcination.

From the measurements of obvious pore channels, the average pore size of HAp samples P123-C, F127-C and P123/F127-C is estimated to be approximately 4.0, 5.3 and 5.2 nm respectively. From the axial view of pore structure, HAp samples do not show precise ordered orientation of the mesopores, generally in a random arrangement. However, through the parallel view, the pores channels are observed to form within the particles, confirming the presence of ordered interconnected pore structures (good pore regularity) which is a typical pore characteristic resulting from self-assembly mechanism of non-ionic surfactants.

The pore size of F127-C is larger than that of P123-C because surfactant F127 ($EO_{100}PO_{70}$ EO_{100}) has more EO portion in its molecular chain than P123 ($EO_{20}PO_{70}EO_{20}$). This results in a much larger EO corona in the micelle structure during the condensation process. This large EO corona therefore leads to a larger pore size. As this ‘‘giant’’ EO corona of F127 is very large, it could not be easily ‘‘squeezed’’ into a perfect ‘‘ball,’’ compared to the smaller EO corona of P123.

The pore channels were able to be formed within the particles and also show the presence of ordered interconnected pore structures (good pore regularity) which is a typical pore characteristic resulted from self-assembly mechanism of non-ionic surfactant.

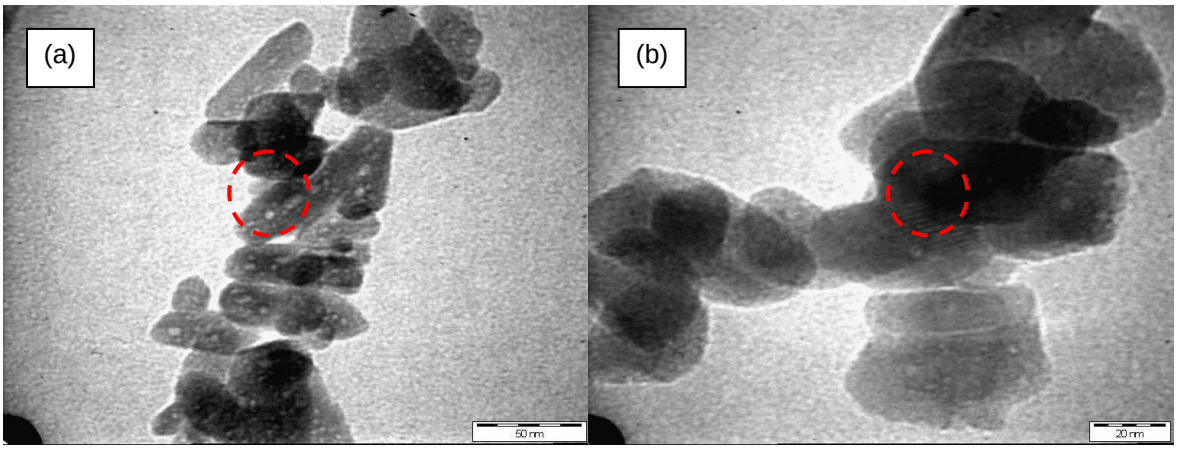

Figure 6. TEM image P123-C (a) axial view, (b) parallel view

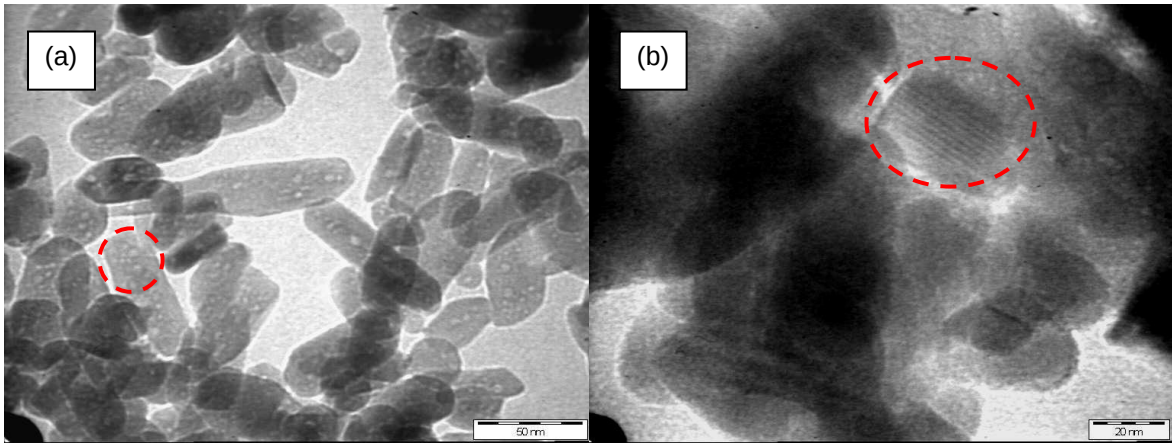

Figure 7. TEM image of F127-C (a) axial view, (b) parallel view

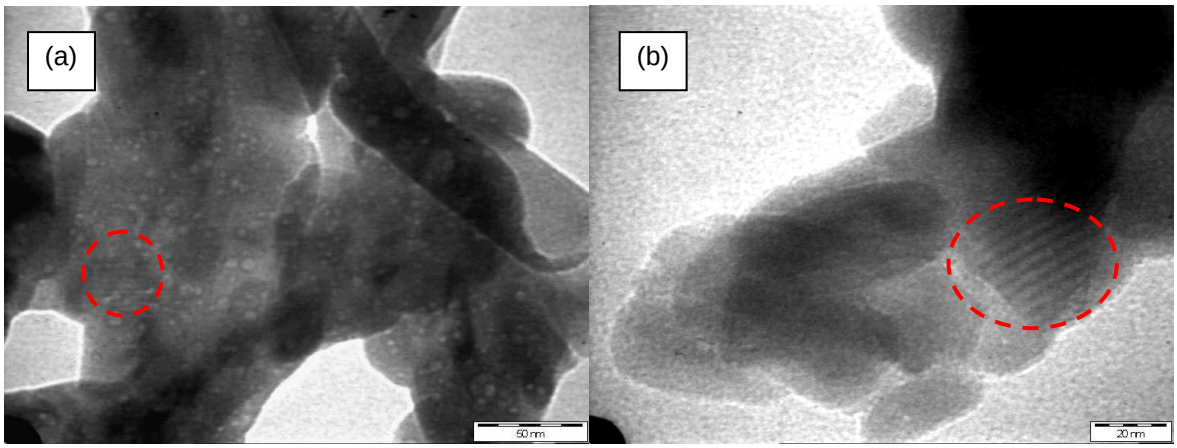

Figure 8. TEM image of F127/P123-C (a) axial view, (b) parallel view

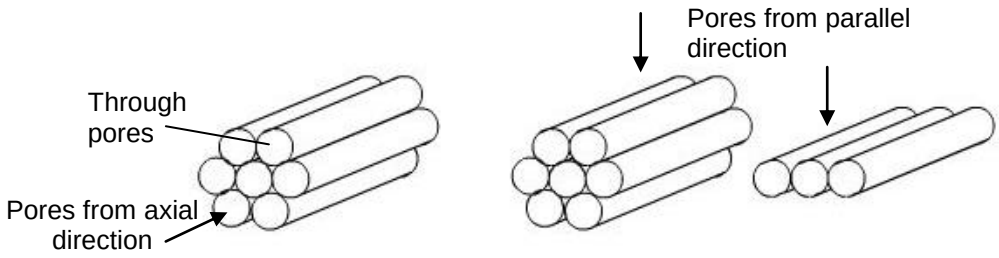

Figure 9. HAp particle observed from different direction with varying view structure of pores (a) axial view, (b) parallel view

The nitrogen adsorption–desorption isotherms (Figure 10) of P123, F127 and P123/F127 samples exhibit type IV curve with a hysteresis loop, and a well defined step at approximately P/P0 = 0.89 – 0.98, implying a broad pore size distribution which is often observed with aggregates plate like particle that give rise to slip shaped pores. This

indicates the presence of ink-bottle type mesopores. The specific surface areas of P123, F127 and P123/F127 calculated based on the BET equation are 48.1, 21.1 and 10.4 m2/g respectively.

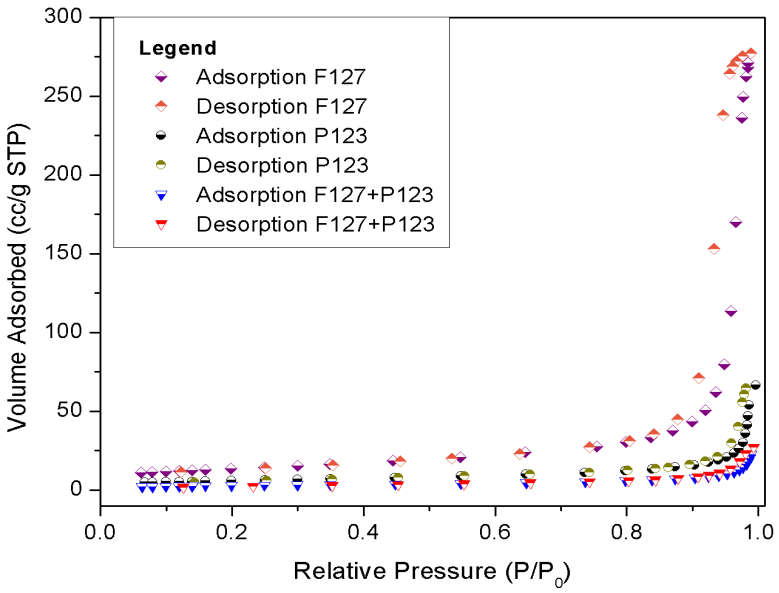

Figure 10. Nitrogen adsorption-desorption isotherm for P123-C, F127-C and P123/F127-C

The mesoporous HA samples that synthesized by using P123, F127 and P123/F127 have average pore size of (BJH Desorption Average Pore Diameter (4V/A)) 27.2, 19.0, and 15.2 nm respectively. The distribution of pore diameters was plotted according to the BJH nitrogen desorption model as shown in Figure 11, 12 and 13. It can be seen from Figure 12 that a broad peak ranging from 10 to 50 nm, centered at about 30 nm, suggesting that most pores are sized at about 30 nm, but the pores are not uniform on the whole. Samples P123 and P123/F127 have 40 nm and 19 nm pore diameter respectively. The reason is that the sizes of pores left by decomposition of the "organic" Pluronics templating structure are not the same as that of the precursor salt. Nevertheless, the pore sizes synthesized by 3 sets of HAp samples generally matches the IUPAC definition for mesopores (2-50 nm).

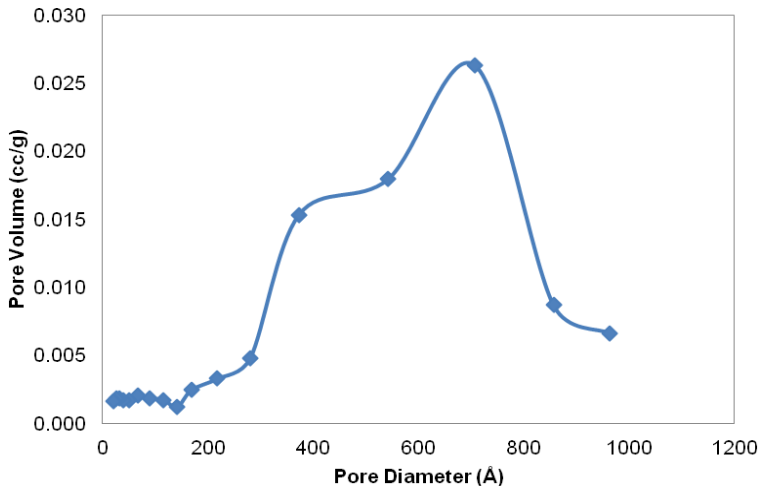

Figure 11. Pore size distribution curve from the desorption for P123

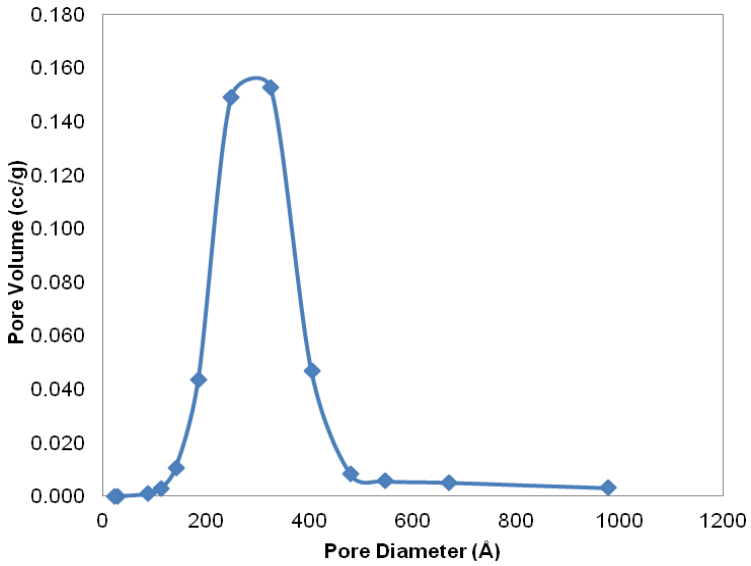

Figure 12. Pore size distribution curve from the desorption for F127

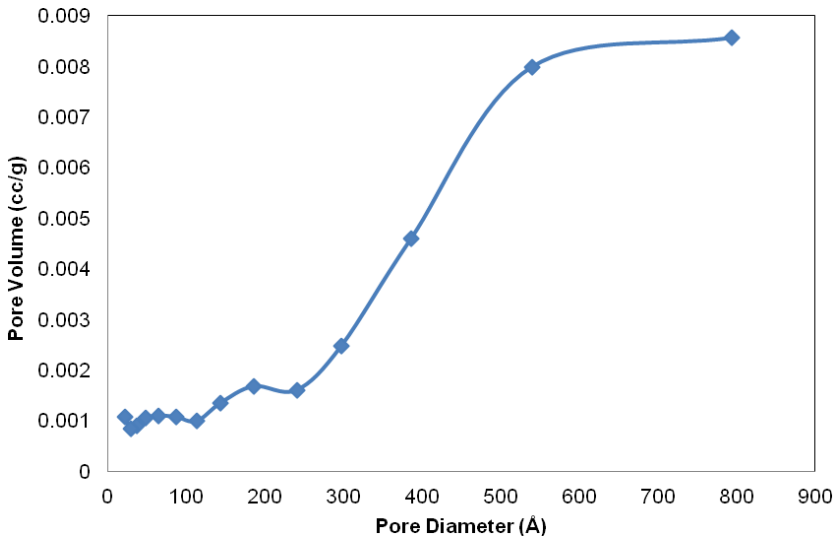

Figure 13. Pore size distribution curve from the desorption for P123 + F127

Conclusions

Mesoporous HAp was successfully synthesized using surfactants P123, F127 and P123 + F127. The mixture of P123 + F127 surfactants for synthesis resulted in HAp with reduced crystallinity, evidently highly suitable to be used as a drug delivery agent. With known pore characteristics and size of synthesized HAp, drugs requiring delivery agents of average pore size 27.2, 19.0, and 15.2 nm could be paired up to produce efficient on-site drug release.

Acknowledgement

Authors would like to thank BASF Malaysia for providing Pluronic samples P123 and F127 used in the present study.

References

[1] M. Akao, H. Aoki, and K. Kato, "Mechanical properties of sintered hydroxyapatite for prosthetic applications," *Journal of Materials Science*, Vol. 16, No. 3, pp. 809-812, 1981.

[2] D.A. Puleo, and A. Nanci, "Understanding and controlling the bone-implant interface," *Biomaterials*, Vol. 20, No. 23-24, pp. 2311-2321, 1999.

[3] A.E. Porter, N. Patel, J.N. Skepper, S.M. Best, and W. Bonfield, "Effect of sintered silicate-substituted hydroxyapatite on remodelling processes at the bone-implant interface," *Biomaterials*, Vol. 25, No. 16, pp. 3303-3314, 2004.

[4] T.J. Gao, T.S. Lindholm, B. Kommonen, P. Ragni, A. Paronzini, and T.C. Lindholm, "Microscopic evaluation of bone-implant contact between hydroxyapatite, bioactive glass and tricalcium phosphate implanted in sheep diaphyseal defects," *Biomaterials*, Vol. 16, No. 15, pp. 1175-1179, 1995.

[5] Y. Mizushima, T. Ikoma, J. Tanaka, K. Hoshi, T. Ishihara, Y. Ogawa, and A. Ueno, "Injectable porous hydroxyapatite microparticles as a new carrier for protein and lipophilic drugs," *Journal of Controlled Release*, Vol. 110, No. 2, pp. 260-265, 2006.

[6] J. Yao, W. Tjandra, Y.Z. Chen, K.C. Tam, J. Ma, and B. Soh, "Hydroxyapatite nanostructure material derived using cationic surfactant as a template," *Journal of Materials Chemistry*, Vol. 13, No. 12, pp. 3053-3057, 2003.

[7] M. Descamps, J.C. Hornez, and A. Leriche, "Manufacture of hydroxyapatite beads for medical applications," *Journal of the European Ceramic Society*, Vol. 29, No. 3, pp. 369-375, 2009.

[8] T.Y. Liu, S.Y. Chen, D.M. Liu, and S.C. Liou, "On the study of BSA-loaded calcium-deficient hydroxyapatite nano-carriers for controlled drug delivery," *Journal of Controlled Release*, Vol. 107, No. 1, pp. 112-121, 2005.

[9] S.P. Victor, and C.P. Sharma, "Development and evaluation of cyclodextrin complexed hydroxyapatite nanoparticles for preferential albumin adsorption," *Colloids and Surfaces B: Biointerfaces*, Vol. 85, No. 2, 2011.

[10] M.P. Ginebra, T. Traykova, and J.A. Planell, "Calcium phosphate cements as bone drug delivery systems: A review," *Journal of Controlled Release*, Vol. 113, No. 2, pp. 102-110, 2006.

[11] H. Zhang, Y. Wang, Y. Yan, and S. Li, "Precipitation of biocompatible hydroxyapatite whiskers from moderately acid solution," *Ceramics International*, Vol. 29, No. 4, pp. 413-418, 2003.

[12] G. Zhang, J. Chen, S. Yang, Q. Yu, Z. Wang, and Q. Zhang, "Preparation of amino-acid-regulated hydroxyapatite particles by hydrothermal method," *Materials Letters*, Vol. 65, No. 3, pp. 572-574, 2011.

[13] M. Toriyama, A. Ravaglioli, A. Krajewski, G. Celotti, and A. Piancastelli, "Synthesis of hydroxyapatite-based powders by mechano-chemical method and their sintering," *Journal of the European Ceramic Society*, Vol. 16, No. 4, pp. 429-436, 1996.

[14] Y.F. Zhao, and J. Ma, "Triblock co-polymer templating synthesis of mesostructured hydroxyapatite," *Microporous and Mesoporous Materials*, Vol. 87, No. 2, pp. 110-117, 2005.

[15] H. Wang, L. Zhai, Y. Li, and T. Shi, "Preparation of irregular mesoporous hydroxyapatite," *Materials Research Bulletin*, Vol. 43, No. 6, pp. 1607-1614, 2008.

[16] G.J. de A.A. Soler-Illia, E.L. Crepaldi, D. Grosso, and C. Sanchez, "Block copolymer-templated mesoporous oxides," *Current Opinion in Colloid & Interface Science*, Vol. 8, No. 1, pp. 109-126, 2003.
[17] C.E. Stevens, "Nonionic surfactants," *Journal of the American Oil Chemists' Society*, Vol. 34, No. 4, pp. 181-185, 1957.
[18] R. Trommer, L. Santos, and C. Bergmann, "Nanostructured hydroxyapatite powders produced by a flame-based technique," *Materials Science and Engineering C*, Vol. 29, No. 6, pp. 1770-1775, 2009.